PCCP

ROYAL SOCIETY OF CHEMISTRY

PAPER

View Article Online
View Journal | View Issue

Cite this: *Phys. Chem. Chem. Phys.*, 2024, **26**, 20908

Synthesis, photophysics and two-photon absorption of imidazole-centred tripodal chromophores†

Jiří Kulhánek, [a] Zuzana Burešová, [a] Milan Klikar, [a] Lampros Sdralias,[b] Alexandros Katsidas,[b] Oldřich Pytela,[a] Patrik Pařík, [a] Aleš Růžička, [c] Mihalis Fakis *[b] and Filip Bureš *[a]

Received 30th May 2024,
Accepted 10th July 2024

DOI: 10.1039/d4cp02227k

rsc.li/pccp

Tripodal push–pull chromophores with D–(π–A)$_3$ arrangement were synthesized using 1-methyl-2,4,5-triphenyl-1*H*-imidazole as a central electron donor, and their thermal, electrochemical, photophysical and non-linear optical properties were studied and corroborated with quantum-chemical calculations. Their facile synthesis involved Suzuki–Miyaura and Knoevenagel reactions, allowing the installation of various peripheral electron acceptors such as formyl, cyano, ester, trifluoromethyl and more complex moieties such as malonic/acetic acid derivatives, indan-1,3-dione and rhodanine. All phenyl rings appended at the central imidazole core were more or less twisted depending on the peripheral substitution. Although imidazole undergoes reversible one-electron oxidation, peripheral acceptors are reduced irreversibly in a multi-electron process. This behaviour is further seen as a variation of the LUMO, while the HOMO remained almost unaltered across the whole series. TD-DFT calculations revealed centrifugal charge transfer from the central imidazole to all C2, C4 and C5 branches occupied by the LUMO, LUMO+1 and LUMO+2. The HOMO–LUMO gap is tuneable within the range of 3.55–2.31 eV, while the longest-wavelength absorption/emission maxima were found within the broad range of 304–448/393–612 nm. Although the absorption spectra are solvent-independent, the emission depends strongly on the solvent polarity and the electron-withdrawing power of the peripheral acceptors. Extended chromophores with complex electron acceptors were investigated as two-photon absorbers, revealing relatively good cross-section values of up to 521 GM and a figure-of-merit ($\Phi_F \times \delta_{2PA}$) of around 190 GM.

Introduction

Linear (D–π–A), dipodal ((D–π)$_2$–A/(A–π)$_2$–D) and tripodal ((D–π)$_3$–A/(A–π)$_3$–D) push–pull chromophores continue to attract steady attention due to their peculiar (optical) properties dictated mostly by the extent of intramolecular charge transfer (ICT) from the donor (D) to the acceptor (A).[1] In principle, di- and tri-podal molecules can adopt either donor- or acceptor-centred arrangements (centrifugal/centripetal; Fig. 1), while these push–pull systems may resemble letters of the alphabet.[2] The central acceptor is mostly represented by aromatic six-membered (hetero)cycles such as 1,3,5-trisubstuted benzene,[3–6] unsymmetrical pyridine,[7,8] diazines[9–13] or symmetrical triazines.[14–16] Tripodal T-shaped chromophores can also be built on indandione central acceptors.[17–19] However, centrifugal chromophores are more frequent, especially those based on triphenylamine cores trisubstituted with peripheral acceptors.[20–24] *N*-Phenylcarbazoles[25] and *N*-heterotriangulenes,[26] representing planarized triphenylamines, can also be used as useful scaffolds to construct tripodal chromophores. Five-membered 1*H*-imidazole can be principally employed as an electron-rich heterocycle, while its 2,4,5-trisubstitution affords tripodal systems.[27] In our former investigation, we utilized 2-substituted imidazole-4,5-dicarbonitrile[28–31] and bis(4-(*N*,*N*-dimethylamino)phenyl)imidazole[32–34] either as electron-withdrawing or -releasing moieties of various Y-shaped push–pull molecules. Hence, modulation of the appended substituents[1] or eventual *N*-quaternization towards (benz)imidazolium (Fig. 1)[35] can significantly affect the imidazole electron properties.

[a] *Institute of Organic Chemistry and Technology, Faculty of Chemical Technology, University of Pardubice, Studentská 573, Pardubice, 53210, Czech Republic. E-mail: filip.bures@upce.cz; Web: https://bures.upce.cz; Tel: +420 46 603 7099*
[b] *Department of Physics, University of Patras, Patras, 26504, Greece. E-mail: fakis@upatras.gr; Tel: +30 2610 996794*
[c] *Department of General and Inorganic Chemistry, Faculty of Chemical Technology, University of Pardubice, Studentská 573, Pardubice, 53210, Czech Republic*

† Electronic supplementary information (ESI) available: Synthesis, NMR spectra, X-ray data, thermal analysis, electrochemistry, optical properties, and DFT data. CCDC 2331438. For ESI and crystallographic data in CIF or other electronic format, see DOI: https://doi.org/10.1039/d4cp02227k

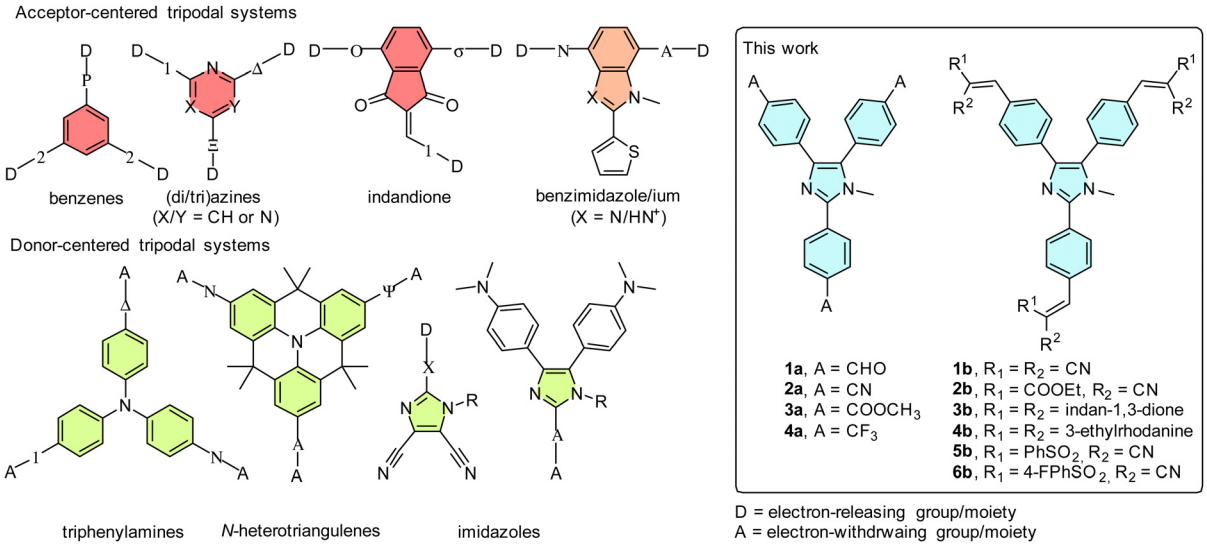

Fig. 1 The most explored acceptor- and donor-centred tripodal push–pull systems along with the general structure of lophine-derived derivatives **1**–**6**.

Imidazole-centred tripodal molecules have found various applications as pharmacophores,[36] charge-transfer (CT) chromophores,[37] fluorophores,[38–42] molecular sensors capable of detecting various analytes such as F^-, BF_4^-/ClO_4^-, Hg^{2+}, Zn^{2+}, cysteine or picric acid,[43–51] viscosity probes,[52] pH probes,[53,54] luminescent solar concentrators (LSCs),[55] emitters for organic light-emitting diodes (OLEDs)[56–59] and robust heterocycles for dye-sensitised solar cells (DSSCs).[60–62] Besides interesting linear optical properties, imidazole push–pull molecules have also been investigated for their nonlinear optical (NLO) activity. For instance, a combination of two ferrocene donors and one ester acceptor imparted imidazole second-order nonlinearity with $\mu_\beta = 780 \times 10^{-48}$ esu, as measured in the EFISH experiment.[63]

N,*N*-Dimethylamino-terminated imidazole-4,5-dicarbonitrile systems showed hyperpolarizability switchable *via* protonation with the hyperpolarizability ratio between the amine ↔ ammonium forms exceeding 20.[31] Imidazole-centred molecules were also utilized as third-order NLOphores, especially for two-photon absorption (2PA). It has been demonstrated that the tripodal Y-shaped arrangement in combination with π-system extension and *N*-substitution allows tuning of the imidazole two-photon absorptivity with 2PA cross-section coefficients δ_{2PA} up to 1700 GM[47,64–73] while molecules with large δ_{2PA} can be applied in applications such as optical limiting,[74,75] photodynamic therapy[76,77] and 2PA-induced microfabrication.[78,79] It is somewhat curious that the 2PA of the parent 2,4,5-triphenylimidazole (lophine) peripherally substituted with electron acceptors has not been addressed so far. Hence, as part of our ongoing efforts towards disclosing the NLO activity of organic fundamental building blocks, such as triphenylamine,[80–83] (di/tri)azines[11,14,82,83] and indan-1,3-dione,[17–19] we report herein the synthesis of two series of lophine-based push–pull chromophores **1**–**6** (Fig. 1) and the investigation of their thermal, electrochemical, linear and third-order NLO properties corroborated with quantum-chemical calculations.

Results and discussion

Synthesis

The synthetic approach towards trisubstituted *N*-methyl lophines **1a**–**4a** is outlined in Scheme 1a.

The synthesis involves threefold Suzuki–Miyaura cross-coupling of 2,4,5-tribromo-1-methylimidazole **1** with 4-substituted phenylboronic acids/pinacol esters **7**–**10** catalysed by $[Pd(PPh_3)_4]$.[84] Chromophores **1a**, **3a** and **4a** were obtained in reasonable 50–80% isolated yields, while the synthesis of tricyano derivative **2a** (25%)

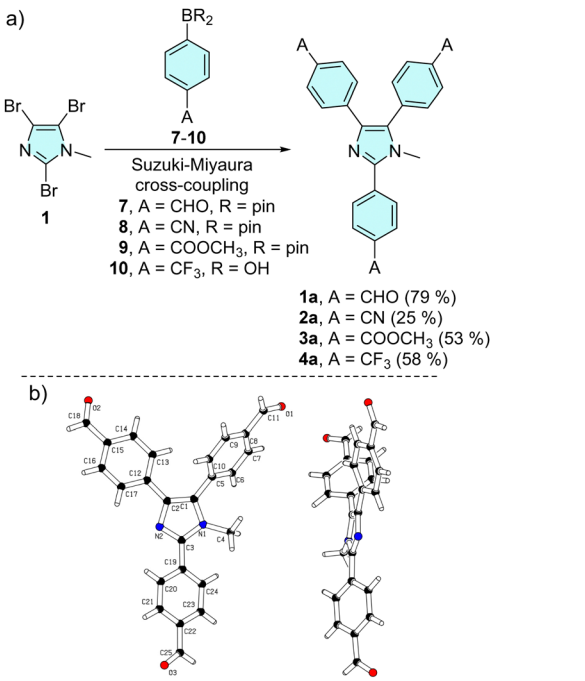

Scheme 1 Threefold cross-coupling reaction of tribromoimidazole towards triphenylimidazole series **a** (a) and X-ray molecular representation (b) of **1a** (CCDC 2331438†).

was accompanied by tedious purification *via* multiple column chromatography. The starting imidazole **1** was prepared by *N*-methylation of commercially available 2,4,5-tribromo-1*H*-imidazole with dimethylsulfate (see the synthesis part in the ESI†).[28]

The molecular structure of tricarbaldehyde **1a** was confirmed by X-ray diffraction (Scheme 1b and Table S1, Fig. S25–S27 in the ESI†). The expected nonplanar arrangement of the central triphenylimidazole corresponds to the related X-ray molecular structures.[39,40,48] For instance, *N*-ethyllophine (CCDC 765921) and **1a** showed a similar nonplanar arrangement of the phenyls appended at the imidazole C2/C4/C5 (torsion angles 41/18/71 *vs.* 27/21/55°). With tricarbaldehyde **1a** in hand, we further extended our investigation to series **b** (Scheme 2). Aldehyde **1a** underwent facile threefold Knoevenagel condensation with activated methylene compounds, such as malonic/acetic acid derivatives **11**–**12**/**15**–**16**, indan-1,3-dione **13** and 3-ethylrhodanine **14**, which allowed the coupling of complex peripheral withdrawing units of various strengths.[85,86] Target chromophores **1b**–**6b** were isolated with yields ranging from 50 to 70%. Knoevenagel condensations using unsymmetrical C-acids **12** and **14**–**16** afforded products **2b** and **4b**–**6b** with an exclusive stereochemistry. Three separate signals of the three vinylic protons found in the ^{1}H-NMR spectra point to a single isomer (Fig. S11, S15, S17 and S19, ESI†). Appropriate configuration assignment was accomplished *via* proton-coupled ^{13}C-NMR spectroscopy allowing the determination of ^{3}J(C–H) interaction constants of the vinylic proton and the neighbouring cyano (**2b**, **5b**, **6b**) and carbonyl (**4b**) carbon atoms (Fig. S21–S24, ESI†). A ^{3}J(C–H) of 13.8 Hz was found for **2b**, **5b** and **6b**, indicating their (*E*)-configuration and chromophore **4b** showed ^{3}J(C–H) = 6.3 Hz pointing to the (*Z*)-isomer.[87]

Thermal analysis

The thermal properties of imidazoles **1**–**6** were determined using differential scanning calorimetry. The native DSC thermograms, deduced melting points T_m and temperatures of thermal decomposition T_d are provided in the ESI† (Fig. S28–S30 and Table S2). With the same central imidazole, the thermal properties of **1**–**6** are dictated by the peripheral withdrawing substituents, and their nature clearly affects the thermal robustness of particular imidazole derivatives. Lophines **1a**–**4a** terminated by fundamental acceptors exhibited a distinctive endothermic melting process between 166 and 273 °C (ester **3a** → nitrile **2a**). Aldehyde **1a** showed two melting peaks, probably due to the presence of a second minor crystalline form. Further heating of the melts of **1a**–**4a** resulted in either evaporation or thermal decomposition of the sample. Trifluoromethyl derivative **4a** was completely evaporated above 380 °C with no apparent residue in the crucible after measurement. In contrast, a neat exothermic decomposition peak was recorded for aldehyde **1a** above 290 °C. Gradual evaporation of the melts of **2a** and **3a** was not observed, and these samples thermally degraded at temperatures above 400 °C. Although nitrile **2a** gradually degraded in a typical exothermic direction, ester **3a** decomposed vigorously endothermically with a clear charred residue in the crucible after analysis. The highest thermal robustness with T_m = 273 °C and T_d > 400 °C was observed for nitrile derivative **2a**.

Imidazole derivatives in series **b** with extended acceptor units afforded more complex thermograms, while a distinct and sharp peak of melting was observed only for cyanoester derivative **2b** (T_m = 196 °C). Compound **6b** underwent a broad and blurred melting process, which was further confirmed visually by measuring the sample in a capillary.

In contrast, no melting was visually observed for indandione derivative **3b**, while the broad endothermic peak above 300 °C was probably related to an enantiotropic solid–solid transition following glass transition at around 270 °C. The other molecules **1b**, **4b** and **5b** decomposed directly without melting. The endothermic peak of **1b** between 180 and 210 °C is probably associated with the solid–solid transition. In general, the molecules with olefinic π-linkers in series **b** showed distinct thermal degradation ranging between 260 and 330 °C.

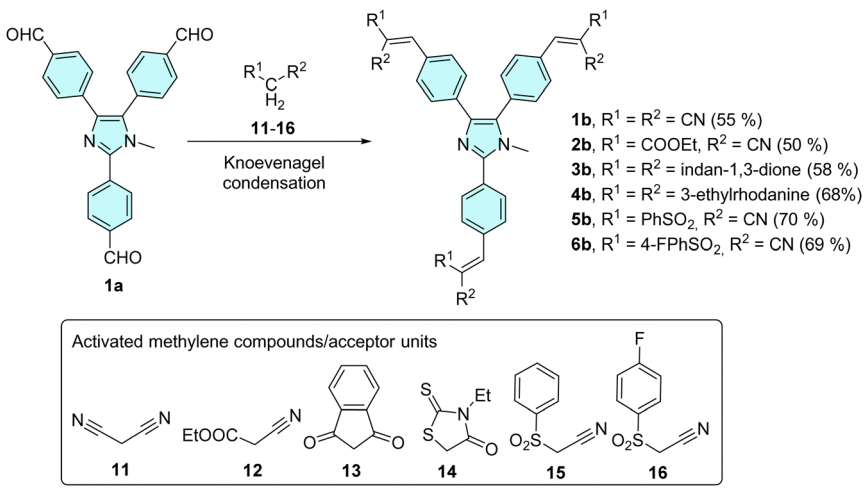

Scheme 2 Knoevenagel condensation of tricarbaldehyde **1a** with various electron-withdrawing moieties towards extended chromophores in series **b**.

Only rhodanine derivative **4b** exhibited a very gradual exothermic decomposition with a hardly distinguishable onset, probably above 220 °C. Nevertheless, the sample was obviously carbonized in a crucible after the DSC analysis. Overall, the thermal stability of the imidazoles in series **a** is higher as compared to those of the extended derivatives in series **b**, which is in line with our previous observations.[19,88]

Electrochemistry

The electrochemical behaviour of the target imidazoles **1–6** was investigated in acetonitrile (ACN) containing 0.1 M Bu_4NPF_6 in a three-electrode cell by cyclic voltammetry (CV). The recorded peak potentials are plotted *vs.* the silver/silver chloride electrode (SSCE). The acquired electrochemical data are summarized in Table 1, and further experimental details and CV diagrams are given in the ESI† (Fig. S31–S39). Indan-1,3-dione derivative **3b** was poorly soluble in ACN and other solvents and, therefore, it was excluded from the CV analysis. The first oxidation of imidazoles **1–6**, except for **4b**, was detected as a reversible process localized on the *N*-methylimidazole unit. The corresponding values of peak-to-peak separation (ΔE_p ~60–70 mV) imply one-electron oxidation. These observations are consistent with the reported electrochemical behaviour of *N*-methyltriphenylimidazole redox catalysts.[89–91] The first oxidation of the rhodanine derivative **4b** was recorded as a fully irreversible process due to the preferential oxidation of the sulphur atom instead of the imidazole, which is consistent with our previous studies.[85,86] The first reduction involves peripheral acceptors and, therefore, it was observed as a multi-electron irreversible process followed by further reductions. This corresponds to the D–(π–A)$_3$ arrangement of the investigated chromophores bearing three unequivocal branches (acceptors). A (quasi)reversible first reduction was observed only for compounds **2a** and **3a** bearing CN and $COOCH_3$ acceptors. The current maxima generally imply that the first reduction is a two-electron process, but more than 10 electrons were exchanged during the reduction of **4a** terminated with trifluoromethyl groups.

Since half-wave potentials are not available for all molecules, the peak potentials E_p^a(ox1) and E_p^c(red1) were used to consistently calculate the HOMO and LUMO energies (Table 1). The $E_{HOMO/LUMO}$ energies, ranging between −6.26 and −5.92/−3.75 and −2.43 eV, are shown in Fig. 2. Except for rhodanine derivative **4b** (E_{HOMO} = −5.92 eV), the E_{HOMO} found at around −6.12 eV confirms that imidazole is a central donor in all target compounds. The HOMO is slightly altered, reflecting the electron-withdrawing power of the appended acceptors. For instance, when comparing compounds in series **a**, the CN groups in **2a** deepened the HOMO down to −6.26 eV, as a result of its strongest electronic effect. The Hammett constants σ_p of the CHO/CN/$COOCH_3$/CF_3 substituents (0.42/0.66/0.45/0.54) roughly correspond to their impact on the HOMO levels of **1a–4a** shown in Fig. 2.[1] The LUMO levels clearly reflect the variation of the peripheral acceptors attached to the lophine core and their readiness towards electrochemical reduction as well as further extension of the π-system. Hence, tricarbaldehyde **1a** proved to be the most easily reducible, followed by cyano, methoxycarbonyl and trifluormethyl derivatives **2a–4a**. More complex acceptor moieties in conjunction with the additional olefinic linker induced a significant deepening of the LUMO levels, thus resulting in a diminished HOMO–LUMO gap compared to series **a**. Although the Δ*E* values of **1a–4a** range between 3.67 and 3.07 eV, the gap of **1b–6b** was found at around 2.45 eV (excluding **4b** with the overestimated HOMO level). Hence, there is not much difference in attaching various

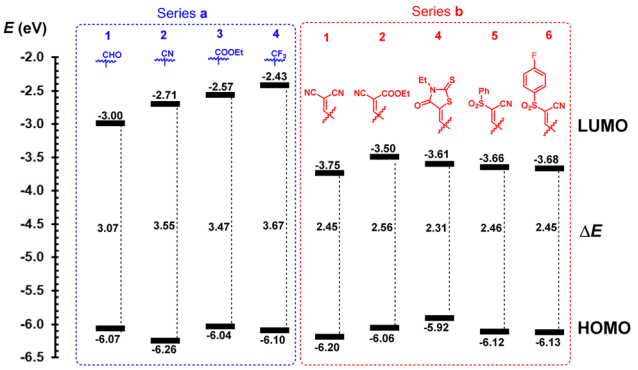

Fig. 2 Energy level diagram of investigated imidazoles **1–6**.

Table 1 Electrochemical data of investigated imidazoles **1–6** measured in ACN (0.1 M Bu_4NPF_6)

Comp.	E_p^a(ox1)[a] [V]	E_p^c(ox1)[a] [V]	E_p^c(red1)[b] [V]	E_p^a(red1)[b] [V]	E_{HOMO}[e] [eV]	E_{LUMO}[e] [eV]	ΔE[f] [eV]
1a	1.60	1.54	−1.47	—[c]	−6.07	−3.00	3.07
2a	1.79	1.72	−1.76	−1.63	−6.26	−2.71	3.55
3a	1.57	1.50	−1.90	−1.80	−6.04	−2.57	3.47
4a	1.63	1.57	−2.04	—[c]	−6.10	−2.43	3.67
1b	1.73	1.66	−0.72	—[c]	−6.20	−3.75	2.45
2b	1.59	1.52	−0.97	—[c]	−6.06	−3.50	2.56
4b	1.45	—[c]	−0.86[d]	—[c]	−5.92	−3.61	2.31
5b	1.65	1.58	−0.81	—[c]	−6.12	−3.66	2.46
6b	1.66	1.59	−0.79	—[c]	−6.13	−3.68	2.45

[a] E_p^a and E_p^c are anodic and cathodic peak potentials of the first reversible oxidation process, respectively. [b] E_p^a and E_p^c are anodic and cathodic peak potentials of the first reversible reduction process, respectively. All CVs were measured at a scan rate of 100 mV s^{-1}, and all potentials were given *vs.* SSCE. [c] Irreversible process. [d] Deducted as a shoulder potential. [e] Energies of the HOMO/LUMO levels calculated according to $-E_{HOMO/LUMO}$ = (E_p^a(ox1) + 0.036) or (E_p^c(red1) + 0.036) + 4.429 (*vs.* SCE).[92,93] The increment of +0.036 V corresponds to the difference between SCE (0.241 *vs.* SHE) and SSCE (0.205 *vs.* SHE). [f] HOMO–LUMO gap $\Delta E = |E_{HOMO} - E_{HOMO}|$ resp. E_p^a(ox1) − E_p^c(red1).

acceptor moieties to the *N*-methyllophine core *via* an additional olefinic linker as in **1b–6b**.

Some differences can be seen in replacing one CN with $COOCH_3$ (**1b** *vs.* **2b**, ΔE = 2.45 *vs.* 2.56 eV), but the presence of an additional fluorine atom in **6b** is diminished compared to **5b** (ΔE = 2.45 *vs.* 2.46 eV).

Linear optical properties

The fundamental optical properties of chromophores **1–6** were investigated *via* electronic absorption and emission spectra measured in four solvents of different polarities (toluene, $CHCl_3$, THF, and ACN; $c = 1 \times 10^{-5}$ M). Fig. 3 and Table 2 show representative spectra/data in THF; see the ESI† for a complete list of spectra (Fig. S41–S44) and data (Tables S3–S5). When going from less polar toluene to more polar ACN, the longest-wavelength absorption band slightly shifts hypsochromically ($\Delta\lambda_{max}$ = 0–10 nm), a typical feature of CT chromophores.[1] The absorption spectra of imidazoles in series **a** exhibit one single band, whereas the spectra of derivatives in series **b** feature two bands and a significantly increased molar absorption coefficient. As demonstrated in Fig. 3a, chromophore **2a** exhibits one absorption band in the UV area (λ_{max} = 325 nm; ε = 32 100 M^{-1} cm^{-1}), whereas its extended analogue **1b** features two bands appearing at 303 (ε = 51 900 M^{-1} cm^{-1}) and 411 nm (ε = 70 000 M^{-1} cm^{-1}). Variation of the acceptor moiety in **1a–4a** and **1b–6b** (Table 2) allowed the tuning of the absorption maxima within the ranges of 304–344 and 399–448 nm, respectively. The measured longest-wavelength absorption maxima vary with different peripheral acceptor substitutions in the same way as observed by electrochemistry. The correlation between the measured optical ($1240/\lambda^{A}_{max}$) and electrochemical gaps (ΔE) is almost perfectly linear with R^2 = 0.99 (see Fig. S40 in the ESI†).

The longest-wavelength absorption band of rhodanine-terminated imidazole **4b** features an additional high-energy shoulder as well as the largest molar absorption coefficient in all used solvents (Fig. 3b). This feature was previously observed for rhodanine molecules[95,96] and can be attributed to the formation of H-aggregates, which is further supported by the diminished fluorescence of **4b**. Indan-1,3-dione acceptors in **3b** induced the most bathochromic shift among all acceptors used, which is in line with our recent study.[85] Analogous to the aforementioned electrochemical measurements, the introduction of a fluorine atom (**5b** → **6b**) has no effect.

In contrast to the steady absorption spectra, the fluorescence spectra (Fig. 3c) are solvent-dependent and red-shifted with increasing solvent polarity (see Fig. S41–S44 in the ESI†). For example, the emission maximum (λ^{E}_{max}) of **1b** shifts from 517 nm in toluene to 617 nm in ACN. The Stokes shifts range between 5.000–9.000 cm^{-1} and increase in the series of solvents

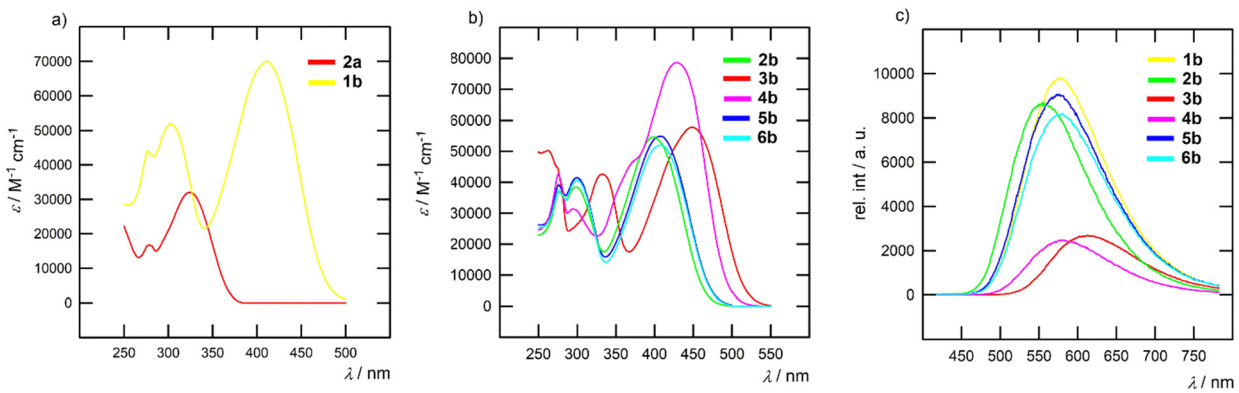

Fig. 3 Representative absorption (a) and (b) and emission (c) spectra of the imidazole chromophores measured in THF.

Table 2 Optical properties of imidazole-centred chromophores **1–6** in THF

Comp.	λ^{A}_{max} [nm eV^{-1}]	ε [M^{-1} cm^{-1}]	λ^{E}_{max} [a] [nm eV^{-1}]	Φ [b] [%]	Stokes shift [cm^{-1} eV^{-1}]	$\langle\tau\rangle$ [c] [ns]	δ_{2PA}[GM]/λ^{max}_{2PA} [nm]	$\Phi_F \times \delta_{2PA}$ [GM]
1a	344/3.60	35 300	452/2.74	17	7000/0.86	—	—	—
2a	325/3.82	32 100	421/2.95	36	7019/0.87	—	—	—
3a	327/3.79	32 300	426/2.91	34	7110/0.88	—	—	—
4a	304/4.08	23 000	393/3.16	32	7440/0.92	—	—	—
1b	411/3.02	70 000	576/2.15	55	7330/0.87	2.04	286/760	157
2b	399/3.11	54 700	554/2.24	56	7010/0.87	2.82	340/740	190
3b	448/2.77	57 800	612/2.03	21	5980/0.74	1.36	286/810	60
4b	429/2.89	78 600	580/2.14	17	6070/0.75	1.34	521/750	88
5b	409/3.03	54 900	573/2.16	52	7000/0.87	2.76	325/750	169
6b	408/3.04	52 000	578/2.15	50	7210/0.89	3.23	390/740	195

[a] Excited at λ^{A}_{max}. [b] Relative to anthracene/perylene (Φ = 0.36/0.94 in cyclohexane)[94] for series **a**/**b**. [c] Average lifetime calculated using nanosecond fluorescence decay $\langle\tau\rangle = \sum A_i\tau_i / \sum A_i$.

in the following order: ACN > THF > $CHCl_3$ > toluene. Hence, we can assume a significant structural re-arrangement of **1**–**6** upon excitation and more polar excited states stabilized by polar solvents. The quantum yields of imidazoles in series **a** showed minor solvent dependency, except for **1a** with increasing Φ_F when going from less polar toluene (Φ_F = 10%) to more polar ACN (Φ_F = 43%). This behaviour is in contrast to that of **1b**–**6b**, whose emission intensity was significantly suppressed with increased solvent polarity. A comparison of the imidazoles in series **b** clearly indicates that increasing the electron-withdrawing power of the appended acceptor results in diminished fluorescence intensity. Fluorescence quenching is especially obvious for indan-1,3-dione and rhodanine derivatives **3b** and **4b**. The pronounced ICT and reduced optical gap in polar solvents offer significant competitive decay pathways, *e.g.* internal conversion and diminishing emissive behaviour of chromophores in series **b**.

To reveal the effect of the electron-withdrawing power of the complex acceptors in **1b**–**6b** on the excited state properties, we performed nanosecond fluorescence dynamics measurements (Fig. 4 and Fig. S45, Tables S6–S9 in the ESI†).

In THF (Fig. 4 and Table S8, ESI†), the decay shows multi-exponential dynamics. Specifically, for **1b** and **4b**, a fast component of 0.2–0.6 ns was found, which is tentatively ascribed to a structural relaxation of the excited state, while two slower components of 1–2 ns and >2 ns were also found in all molecules. For **2b**, **5b** and **6b**, the fluorescence dynamics were detected at various emission wavelengths in order to identify and separate the contribution of the emissive states. For this reason, the decays were fitted using a global method (Fig. S46 and Table S10, ESI†). In these three molecules, the contributions of the fast/slow components (A_1 and A_2, respectively) were found to decrease/increase as the detection wavelength shifted to the low-energy edge of the spectrum. However, these changes are small, and therefore, the two components cannot originate from emissive states of different natures (*e.g.* a locally excited and an ICT state), but they can rather be ascribed to different conformers existing in the elongated compounds in series **b** due to rotation around the quasi-single bonds. The average lifetime ranges from 1.3 to 3.2 ns, which is smaller for **3b** and **4b**. The latter finding is in accordance with the reduced Φ_F in these two chromophores with the strongest indan-1,3-dione and rhodanine electron acceptors, indicating increased non-radiative pathways. The fluorescence decays in all other solvents also present complex multiexponential dynamics, while a common conclusion is that **3b** and **4b** exhibit the fastest dynamics. Besides, on comparing the dynamics in the two non-chlorinated solvents, toluene and THF, it was observed that the lifetime of the slower component increased by increasing the polarity of the solvent from toluene to THF (*e.g.* τ = 2.58 and 3.74 ns in toluene and THF were recorded for **6b**).

This is correlated to an emission from a more relaxed emitting state.[97,98] In the highest polarity solvent, ACN, the lifetime drops significantly due to increased non-radiative transitions followed by a decrease of the energy gap between the final emitting and the ground state.

Two-photon absorption

The 2PA spectra were measured for extended chromophores **1b**–**6b** in toluene and THF (Fig. 5). The maximum δ_{2PA} values in THF are listed in Table 2. Relatively good values were found for all compounds in both solvents, with δ_{2PA} reaching ~350 to 400 GM for chromophores **2b** and **6b** in THF, as well as adequate quantum yield Φ_F. The maximum values, however, were detected for **4b** with rhodanine acceptors, which also possessed a small quantum yield. Consequently, the smallest 2PA action cross-section values, *i.e.* $\Phi_F \times \delta_{2PA}$ were found for **3b** and **4b**, bearing the strongest indan-1,3-dione and rhodanine peripheral acceptors. Larger δ_{2PA} are expected for systems possessing large transition dipole moments and differences in the permanent dipole moments in the ground and final states, with the latter being related to the Stokes shift. Chromophores **1b**–**6b** exhibit significant transition dipole moments while **2b** and **6b** experience the most spread LUMO towards the C5-branch (*vide infra*), which is possibly related to their better 2PA activity. The peaks in the 2PA spectra were observed in the short wavelength region within our experimental range,

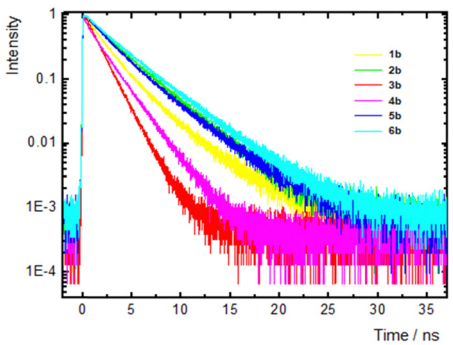

Fig. 4 Fluorescence dynamics on the nanosecond timescale of imidazole chromophores **1b**–**6b** measured in THF. Dynamics were detected at the peaks of the fluorescence spectra.

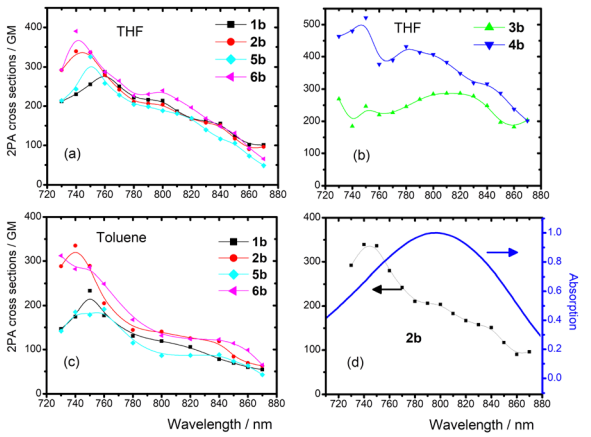

Fig. 5 2PA spectra of compounds **1b**–**6b** in THF (a) and (b) and toluene (c); (d) shows the comparison of the 2PA spectrum *vs.* the rescaled 1PA one for **2b** in THF.

i.e. 730–760 nm. A comparison of the spectral shape and position of the 2PA spectra *vs.* the rescaled 1PA spectra is shown in the inset of Fig. 5d for **2b** in THF. As expected for tripodal compounds, the 2PA peak is obviously hypsochromically shifted with respect to twice the peak wavelength of the 1PA spectrum, indicating that the lower energy state, produced *via* excitonic coupling, is only partially 2-photon allowed while the main contribution to the 2PA originates from the higher energy state. Such a behaviour resembles the one previously found for other triphenylamine- or triazine-centred D–(π–A)$_3$ and A–(π–D)$_3$ chromophores.[14,99,100]

Next, we tried to establish a more quantitative aspect of the effect of the different electron-withdrawing groups by calculating the difference between the permanent dipole moments of the ground and excited states, $\Delta\mu_{2PA}$, using the measured lowest energy peak 2PA cross-sectional values $\delta_{2PA}(0–0)$ and the following relationship:[14,101–103]

$$\Delta\mu_{2PA} = \left(\frac{5}{4(1+2\cos^2\theta)}\frac{hcN_A}{\pi 10^3 \ln 10}\frac{n}{{f_{opt}}^2}\frac{\nu_{max}}{\varepsilon_{max}}\delta_{2PA}(0-0)\right)^{1/2}$$

where ν_{max} is the lowest energy absorption frequency (in Hz), ε_{max} is the peak molar absorption coefficient (in mol^{-1} dm^3 cm^{-1}), θ is the angle between the dipole moments of the excited and ground states (considered as θ = 0), n is the refractive index (1.41 for THF) and f_{opt} is the local field factor equal to $(2 + n^2)/3$. The calculated values are summarized in Table S11 (ESI†) and range from 12.8 D for **1b** to 17.4 D for **6b**, being in good similarity with other 2PA chromophores.[14,101,103]

DFT calculations

The spatial and electronic properties of all target derivatives **1–6** were investigated at the DFT level by using the Gaussian® 16 software package.[104] Optimized geometries of the chromophores **1a–4a**/**1b–3b** were calculated using the DFT B3LYP/6-311+G(2d,p) method, while the sulphur-containing structures **4b–6b** were optimized using DFT B3LYP/6-311+G(2df,p). The same methods were used to calculate the energies of the HOMO (E^{DFT}_{HOMO}) and the LUMO (E^{DFT}_{LUMO}), their differences (ΔE^{DFT}) and ground-state dipole moments μ (Table 3).

The optimized geometries shown in Fig. S47 (ESI†) reveal nonplanar arrangement similar to that observed in the solid state by X-ray analysis (Scheme 1). In general, the phenyl ring appended at C5 proved to be most forced out of the imidazole plane because of its repulsion with the neighbouring N–CH$_3$ group. Sulfones **5b** and **6b** show a tetrahedral arrangement of the sulphur atoms, resulting in the most nonplanar molecules. The ground state dipole moment of imidazoles in series **a** is relatively steady (6.74–8.60 D) and extension of the π-system end-capped with peripheral (complex) electron-withdrawing units of various geometries in series **b** resulted in large fluctuations in the dipole moments (5.18–13.12 D, Table 3). The aforementioned nonplanar arrangements of sulfones **5b** and **6b** most likely also account for their large ground state dipole moments. The lowest HOMO–LUMO gap was calculated for **1a** (3.69 eV) and **4b** (2.73 eV), which is in line with the electrochemical measurements (Table 1). In general, the DFT-calculated energies of the HOMO/LUMO are slightly overestimated but the trends seen by electrochemical measurements are clearly observed, as electrochemical and DFT-calculated gaps correlate very tightly (Fig. S51, ESI†).

The electrostatic potentials showed for representative chromophores **1a**/**2a** and **1b**/**3b**/**6b** in Fig. 6 imply that, except for **1a** and **3b**, the central imidazole core is neutrally charged and negative and positive charges appear rather on the peripheral

Table 3 DFT-calculated energies of the frontier molecular orbitals, HOMO–LUMO gap (ΔE^{DFT}), ground state dipole moment (μ), longest-wavelength absorption maxima (λ^A_{max}) and transitions (dipole moment) of imidazoles **1–6** in ACN

Comp	E^{DFT}_{HOMO} [eV]	E^{DFT}_{LUMO} [eV]	ΔE^{DFT} [eV]	μ^b [D]	$\lambda^A_{max}{}^c$ [nm eV^{-1}]	$\lambda^A_{max}{}^d$ [nm eV^{-1}]	Wavelength [nm]: transitions (f); $\mu_{trans}{}^{de}$ [D]
1a	−6.16	−2.47	3.69	8.60	380/3.26	310/4.00	315: H → L/H → L+1 (0.79); 7.25 305: H → L+1 (0.72), 6.85
2a	−6.22	−2.15	4.07	7.65	342/3.63	293/4.23	296: H → L/H → L+1 (0.84); 7.28 290: H → L+1 (0.69); 6.53
3a	−6.06	−2.06	4.00	7.91	349/3.55	292/4.25	298: H → L (0.89); 7.50 289: H → L/H → L+1 (0.69); 6.50
4a	−6.14	−1.70	4.44	6.84	310/4.00	272/4.56	276: H → L+1 (0.59); 5.90 271: H → L/H → L+1 (0.56); 5.70
1b	−6.17	−3.34	2.83	5.18	489/2.54	389/3.19	396: H → L/H → L+1 (0.99); 9.14 384: H → L+1 (1.83); 12.22
2b[a]	−6.04	−3.11	2.93	7.70	482/2.57	379/3.27	386: H → L/H → L+1 (1.03); 9.17 373: H → L+1 (1.87); 12.19
3b	−5.96	−3.23	2.73	6.37	522/2.38	405/3.06	408: H → L (1.15); 10.00 396: H → L/H → L+1 (2.51); 14.53
4b[a]	−5.83	−3.10	2.73	7.81	517/2.40	402/3.08	407: H → L+1 (1.18); 10.08 398: H → L/H → L+1 (2.49); 14.52
5b	−6.12	−3.14	2.98	13.12	477/2.60	376/3.30	381: H → L/H → L+1 (1.13); 9.56 371: H → L+1 (1.89); 12.20
6b	−6.04	−3.05	2.99	9.23	469/2.64	376/3.30	381: H → L/H → L+1 (1.13); 9.55 371: H → L+1 (1.89); 12.20

[a] Calculated as the corresponding methyl ester and 3-methylrhodanine derivatives. [b] Ground state dipole moment. [c] Calculated using the TD-DFT B3LYP/6-311+g(2df,p) method. [d] Calculated using the TD-DFT CAM-B3LYP/6-311+g(2df,p) method. [e] H/L corresponds to the HOMO/LUMO; f is the oscillator strength; and μ_{trans} is the ground to excited state transition dipole moment.

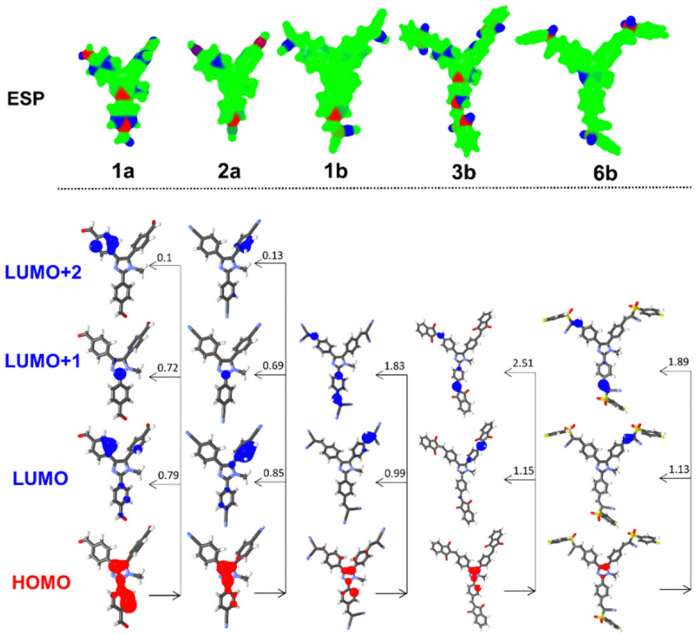

Fig. 6 DFT-calculated ESP charges, the HOMO/LUMO(+1/2) localization, and CT transitions, including oscillator strengths in representative chromophores in series **a** and **b**.

withdrawing groups bearing heteroatoms (see Fig. S48 for complete visualization, ESI†). However, the HOMO/LUMO localization (Fig. 6 and Fig. S49, S50 in the ESI†) reveals the imidazole- and 2-phenylimidazole-centred HOMO and that the LUMO spreads on the appended phenyl rings, the C5-branch in particular. Hence, centrifugal charge separation with a central imidazole donor can be deduced. The calculated energies of the HOMO/LUMO are slightly overestimated, but the trends seen from the electrochemical measurements are clearly obeyed as both quantities correlate very tightly (Fig. S51, ESI†). Considering the identical π-systems in both series **a** (triphenyl-*N*-methylimidazole) and **b** (tri(4-vinylphenyl)-*N*-methylimidazole), the variation of electronic properties must be ascribed to the appended substituents. In series **a**, the calculated LUMO energies roughly correspond to the Hammett constants of the simple CN, $COOCH_3$ and CF_3 substituents (except for **1a**). The influence of peripheral CN, COOEt, indan-1,3-dione, 3-ethylrhodanine, $PhSO_2$ and 4-$FPhSO_2$ substituents is more complex. Due to their various spatial arrangements along the peripheral olefinic linker(s), their electronic effects are differently pronounced. However, sulfones **5b** and **6b** showed a deepened LUMO due to the strong electron-withdrawing power of SO_2Ph (0.68) and, expectedly, even stronger SO_2PhF.

Electronic absorption spectra were predicted using the TD-DFT B3LYP/6-311+g(2df,p) and CAM-B3LYP/6-311+g(2df,p) methods in ACN. Fig. 7 shows the spectra calculated using TD-DFT CAM-B3LYP/6-311+g(2df,p) along with the experimental spectra for the selected chromophores; see Fig. S52 and S53 (ESI†) for complete spectra. Compared with the experimental data in ACN (Fig. S44, ESI†), the spectra calculated using B3LYP/CAM-B3LYP are red/blue-shifted, but the number and shape of the peaks are identical. A correlation of the

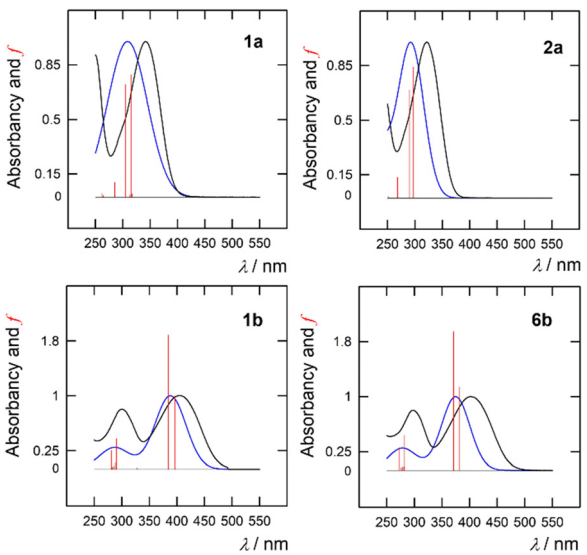

Fig. 7 UV-Vis absorption spectra in ACN calculated using TD-DFT CAM-B3LYP/6-311+g(2df,p) (blue) along with the experimental spectra (black). The red vertical lines represent oscillator strength (*f*).

experimental (Table 2) and calculated (Table 3) optical gaps (calculated as $1240/\lambda^{A}_{max}$) using both functionals is tight (Fig. S54, ESI†), which indicates that both methods are capable of describing trends in the electronic properties of imidazole derivatives **1**–**6**. However, the slope of the regression implies better agreement for the CAM-B3LYP calculated λ^{A}_{max} values (Fig. S54, ESI†).

The single absorption band of imidazoles in series **a** is due to the HOMO → LUMO and HOMO → LUMO+1 transitions (Table 3 and Fig. 6) accompanied by a weaker transition from

the HOMO to the LUMO+2. Extension of the π-system and installation of the complex peripheral acceptors as in series **b** resulted in red-shifted spectra with two particularly evolved absorption bands. The longest-wavelength absorption band is generated by the HOMO → LUMO transition along with the HOMO → LUMO+1 excitation of an even larger oscillator strength. Hence, considering that the LUMO, LUMO+1 and LUMO+2 in **1a**–**4a** spread across all three branches and likewise the LUMO and LUMO+1 in **1b**–**6b** (Fig. 6), we can assume a centrifugal charge transfer from the imidazole-centred HOMO to the peripheral electron acceptors. The transition from the imidazole-centred HOMO to the peripheral branches occupied by the LUMO(+1/2) is accompanied by significant transition dipole moments, which are larger for **1b**–**6b**, as listed in Table 3.

Conclusions

Two series of lophine-based tripodal chromophores were prepared. The synthesis of chromophores **1a**–**4a** involved threefold cross-coupling, while subsequent Knoevenagel condensation allowed the installation of complex peripheral acceptors based on acetic/malonic acids, indan-1,3-dione and rhodanine to afford **1b**–**6b**. Structural analysis revealed a nonplanar arrangement of the central *N*-methyltriphenylimidazole and also exclusive stereochemistry of olefinic chromophores **1b**–**6b**. DFT calculations further identified sulfones **5b** and **6b** as the most nonplanar compounds with the largest ground state dipole moments. The thermal stability measured by DSC was high with the temperature of decomposition ranging between 220 and 400 °C. However, the extension of the π-system diminished thermal stability, and the compounds in series **b** are thus less thermally robust compared to those in series **a**. Electrochemical measurements revealed a reversible one-electron oxidation centred on imidazole, while the irreversible multi-electron reduction involved peripheral acceptor moieties. The D–(π–A)$_3$ arrangement of **1**–**6** further resulted in a steady HOMO and the LUMO reflecting the electron-withdrawing power of the acceptors. The centrifugal ICT from the imidazole-centred HOMO to the peripheral LUMO/LUMO+1/LUMO+2 spread among the branches was further corroborated by TD-DFT calculations. In general, lower HOMO–LUMO gaps were recorded/calculated for extended chromophores in series **b** bearing more powerful electron acceptors and extended π-system. The absorption spectra are solvent-independent while the variation of the acceptor allows tuning of the absorption maxima from 300 to 450 nm. The calculated spectra followed the same trend. In contrast, the fluorescence spectra red-shifted with increasing polarity of the environment and the fluorescence was obviously dependent on the electron-withdrawing power of the peripheral acceptors and solvent polarity. Tripodal imidazoles **1b**–**6b** showed relatively good and tuneable two-photon absorption with δ_{2PA} within the range of 286 to 521 GM. Although the maximum value was measured for rhodanine chromophore **4b**, ester **2b** and sulfone **6b** showed the largest figure of merit ($\Phi_F \times \delta_{2PA}$). The recorded δ_{2PA} values correspond to the reported data for centrifugal imidazole-based chromophores.[65] However, generally, a larger cross-section can be achieved when imidazole is applied as a central π-linker of unsymmetrical D–π–(A)$_2$ or A–π–(D)$_2$ tripodal chromophores.[47,64] The results presented herein demonstrate the profound effect of the ICT process on the photophysics and NLO properties of the imidazole compounds. The strength and dynamics of this process, depending on the molecular structure, architecture and environment, have been the subject of intense scientific research in recent years.[105–107] Due to the positive dipole moment change upon excitation, the excited state is more prone to environmental changes that experience a larger solvent reaction field. Here, molecules with stronger electron-accepting groups exhibit a reduced energy gap, Φ_F and excited state lifetime.

Author contributions

Investigation: JK, ZB, MK, LS, AK, OP, PP and AR; methodology: JK, MF and FB; writing – original draft: FB; writing – review and editing: MF and FB.

Data availability

The data supporting this article have been included as part of the ESI.† Crystallographic data for **1a** has been deposited at the CCDC under 2331438 and can be obtained from **https://www.ccdc.cam.ac.uk**.

Conflicts of interest

There are no conflicts to declare.

References

1 F. Bureš, *RSC Adv.*, 2014, **14**, 58826.
2 M. Klikar, P. Solanke, J. Tydlitát and F. Bureš, *Chem. Rec.*, 2016, **16**, 1886.
3 F. Terenziani, C. Le Droumaguet, C. Katan, O. Mongin and M. Blanchard-Desce, *Chem. Phys. Chem.*, 2007, **6**, 723.
4 B. Mu, X. Quan, Y. Zhao, X. Li and W. Tian, *Mater. Chem. Front.*, 2019, **3**, 1671.
5 S. Pelz, J. Zhang, I. Kanelidis, D. Klink, L. Hyzak, V. Wulf, O. J. Schmitz, J. C. Gasse, R. Frahm, A. Pütz, A. Colsmann, U. Lemmer and E. Holder, *Eur. J. Org. Chem.*, 2013, 4761.
6 T. Shimasaki, Y. Takiyama, Y. Nishihara, A. Morimoto, N. Teramoto and M. Shibata, *Tetrahedron Lett.*, 2015, **56**, 260.
7 C. K. R. Namboodiri, P. B. Bisth, R. Mukkamala, R. Chandra and I. S. Aidhen, *Chem. Phys.*, 2013, **415**, 190.
8 H. F. Huang, S. H. Xu, Y. B. He, C. C. Zhu, H. L. Fan, X. H. Zhou, X. C. Gao and Y. F. Dai, *Dyes Pigm.*, 2013, **96**, 705.
9 S. Achelle, M. Hodeé, J. Massue, A. Fihey and C. Katan, *Dyes Pigm.*, 2022, **200**, 110157.

10 S. Achelle and F. Robin-le Guen, *J. Photochem. Photobiol., A*, 2017, **348**, 281.
11 M. Fecková, P. le Poul, F. Bureš, F. Robin-le Guen and S. Achelle, *Dyes Pigm.*, 2020, **182**, 108659.
12 S. Achelle, J. Rodríguez-López and F. Robin-le Guen, *Org. Biomol. Chem.*, 2023, **21**, 39.
13 S. Achelle, J. Rodríguez-López, F. Bureš and F. Robin-le Guen, *Chem. Rec.*, 2020, **20**, 440.
14 P. Šimon, M. Klikar, Z. Burešová, Ch Vourdaki, A. Katsidas, J. Tydlitát, J. Kulhánek, J. Zelenka, M. Fakis and F. Bureš, *J. Mater. Chem. C*, 2023, **11**, 7252.
15 N. P. Tripathi, S. Jain, R. K. Singh and S. Sengupta, *Chem. - Eur. J.*, 2023, e202303244.
16 A. Maggiore, X. Tan, A. Brosseaus, A. Danos, F. Miomandre, A. P. Monkman, P. Audebert and G. Clavier, *Phys. Chem. Chem. Phys.*, 2022, **24**, 17770.
17 P. Solanke, F. Bureš, O. Pytela, M. Klikar, T. Mikysek, L. Mager, A. Barsella and Z. Růžičková, *Eur. J. Org. Chem.*, 2015, 5339.
18 T. Adhikari, P. Solanke, D. Pathak, T. Wagner, F. Bureš, T. Reed and J. M. Nunzi, *Opt. Mater.*, 2017, **69**, 312.
19 P. Solanke, O. Pytela, F. Bureš and M. Klikar, *Dyes Pigm.*, 2019, **162**, 755.
20 P. Blanchard, C. Malacrida, C. Cabanetos, J. Roncali and S. Ludwigs, *Polym. Int.*, 2019, **68**, 589.
21 A. Karak, S. K. Manna and A. K. Mahapatra, *Anal. Methods*, 2022, **14**, 972.
22 X. Lian, Z. Zhao and D. Cheng, *Mol. Cryst. Liq. Cryst.*, 2017, **648**, 223.
23 A. Mahmood, *Sol. Energy*, 2016, **123**, 127144.
24 H. J. Yen and G. S. Liou, *Polym. Chem.*, 2018, **9**, 3001.
25 L. S. Cui, S. C. Dong, Y. Liu, Q. Li, Z. Q. Jiang and L. S. Liao, *J. Mater. Chem. C*, 2013, **1**, 3967.
26 N. Hammer, T. A. Schaub, U. Meinhardt and M. Kivala, *Chem. Rec.*, 2015, **15**, 1119.
27 J. Kulhánek and F. Bureš, *Beilstein J. Org. Chem.*, 2012, **8**, 25.
28 J. Kulhánek, F. Bureš, O. Pytela, T. Mikysek, J. Ludvík and A. Růžička, *Dyes Pigm.*, 2010, **85**, 57.
29 F. Bureš, J. Kulhánek, T. Mikysek, J. Ludvík and J. Lokaj, *Tetrahedron Lett.*, 2010, **51**, 2055.
30 J. Kulhánek, F. Bureš, W. Kuznik, I. V. Kityk, T. Mikysek and A. Růžička, *Chem. – Asian J.*, 2013, **8**, 465.
31 A. Plaquet, B. Champagne, J. Kulhánek, F. Bureš, E. Bogdan, F. Castet, L. Ducasse and V. Rodriguez, *ChemPhysChem*, 2011, **12**, 3245.
32 J. Kulhánek, F. Bureš, T. Mikysek, J. Ludvík and O. Pytela, *Dyes Pigm.*, 2011, **90**, 48.
33 J. Kulhánek, F. Bureš, O. Pytela, T. Mikysek and J. Ludvík, *Chem. – Asian J.*, 2011, **6**, 1604.
34 N. Dey, J. Kulhánek, F. Bureš and S. Bhattacharya, *J. Org. Chem.*, 2021, **86**, 14663.
35 T. Inouchi, T. Nakashima, M. Toba and T. Kawai, *Chem. – Asian J.*, 2011, **6**, 3020.
36 S. Chettri, S. Tamang, P. Rai, Y. Rai, U. K. Singha, K. Pradhan, D. Brahman and B. Sinha, *J. Heterocyclic Chem.*, 2023, **60**, 1394.
37 A. Patel, F. Bureš, M. Ludwig, J. Kulhánek, O. Pytela and A. Růžička, *Heterocycles*, 2009, **78**, 999.
38 O. L. Al Sharif, L. M. Nhari, R. M. El-Shishtawy and A. M. Asiri, *Mater. Today Chem.*, 2023, **29**, 101453.
39 P. Ganesan, P. Ganesan, Z. Zhang, J. Xu, R. Rajalingam and P. Gao, *J. Org. Chem.*, 2023, **88**, 4077.
40 K. Feng, F. L. Hsu, D. Van DerVeer, K. Bota and X. R. Bu, *J. Photochem. Photobiol., A*, 2004, **165**, 223.
41 H.-N. Peng, Y. Yu, X.-H. Liu, J. Zheng, H. Cheng and X. Hu, *J. Chem. Res.*, 2018, **1**, 20.
42 R. Babar, M. Ali Munawar, M. N. Tahir and M. Arif, *Spectrochim. Acta, Part A*, 2019, **217**, 223.
43 S. S. Razi, R. C. Gupta, R. Ali, S. K. Dwivedi, P. Srivastava and A. Misra, *Sens. Actuators, B*, 2016, **236**, 520.
44 S. Tsuchiya, K. Sakai, K. Kawano, Y. Nakane, T. Kikuchi and T. Akutagawa, *Chem. - Eur. J.*, 2018, **24**, 5868.
45 X. He, S. Zhu, H. Chen, Y. Wang and H. Li, *J. Lumin.*, 2016, **173**, 218.
46 K. G. Harsha, Ch Madhu, N. Puvvada, T. R. Rao Baggi, V. J. Rao and N. R. Chereddy, *Chemistry Select*, 2020, **5**, 6059.
47 M. Zhang, M. Li, Q. Zhao, F. Li, D. Zhang, J. Zhang, T. Yi and Ch Huang, *Tetrahedron Lett.*, 2007, **48**, 2329.
48 T. Khamrang, A. Kathiravan, Ch Ponraj and D. Saravanan, *J. Mol. Struct.*, 2021, **1238**, 130442.
49 C. I. C. Esteves, R. C. M. Ferreira, M. M. M. Raposo and S. P. G. Costa, *Dyes Pigm.*, 2018, **151**, 211.
50 H. E. Okda, S. El Sayed, R. C. M. Ferreira, S. P. G. Costa, M. M. M. Raposo, R. Martínez-Mánez and F. Sancenón, *Dyes Pigm.*, 2018, **159**, 45.
51 H. E. Okda, S. El Sayed, I. Otri, R. C. M. Ferreira, S. P. G. Costa, M. M. M. Raposo, R. Martínez-Mánez and F. Sancenón, *Dyes Pigm.*, 2019, **162**, 303.
52 S. Aryamueang, K. Chansaenpak, A. Watwiangkham, S. Suthirakun, P. Muangsopa, W. Wattanathana, R.-Y. Lai and A. Kamkaew, *J. Photochem. Photobiol., A*, 2024, **447**, 115268.
53 R. P. C. L. Sousa, R. B. Figueira, B. R. Gomes, S. P. G. Costa, M. Azenha, R. F. P. Pereira and M. M. M. Raposo, *RSC Adv.*, 2021, **11**, 24613.
54 R. P. C. L. Sousa, R. B. Figueira, B. R. Gomes, S. Sousa, R. C. M. Ferreira, S. P. G. Costa and M. M. M. Raposo, *Nanomaterials*, 2021, **11**, 3401.
55 E. Rosadoni, F. Bellina, M. Lessi, C. Micheletti, F. Ventura and A. Pucci, *Dyes Pigm.*, 2022, **201**, 110262.
56 G. Li, M. Xia, J. Liu, J. Zheng, B. Zhao and H. Peng, *Dyes Pigm.*, 2023, **213**, 111183.
57 Y.-D. Lin, W.-W. Tsai and C.-W. Lu, *Chem. - Eur. J.*, 2023, **29**, e202203040.
58 G. Umasankar, H. Ulla, Ch Madhu, G. R. Reddy, B. Shanigaram, J. B. Nanubolu, B. Kotamarthi, G. V. Karunakar, M. N. Satyanaryan and V. J. Rao, *J. Mol. Struct.*, 2021, **1236**, 130306.
59 M. Pokladko-Kowar, N. Nosidlak, E. Gondek, I. V. Kityk, F. Bureš F, J. Kulhánek and P. Karasinski, *Opt. Quantum Electron.*, 2016, **48**, 82.

60 D. Unny, G. R. Kandregula and K. Ramanujan, *J. Photochem. Photobiol., A*, 2022, **426**, 113735.
61 J. Sivanadanam, I. Aldhen and K. Ramanujam, *New. J. Chem.*, 2020, **44**, 10207.
62 M. Velusamy, Y.-C. Hsu, J. T. Lin, C.-W. Chang and C.-P. Hsu, *Chem. – Asian J.*, 2010, **5**, 87.
63 S. Prabu, F. Francesco, A. Colombo, C. Dragonetti, P. Biagini, F. Melchiorre and N. Palanisami, *New J. Chem.*, 2024, **48**, 394.
64 K. Feng, L. De Boni, L. Misoguti, C. R. Mendonca, M. Meador, F. L. Hsu and X. R. Bu, *Chem. Commun.*, 2004, 1178.
65 G. C. Zheng, Z. B. Cai, Y. L. Pan, L. Bai, Y. T. Zhou, S. L. Li and Y. P. Tian, *Tetrahedron*, 2016, **72**, 2988.
66 Z. B. Cai, Q. X. Lou, S. L. Li, L. J. Chen, Q. Ye and Y. P. Tian, *Analyst*, 2022, **147**, 5495.
67 K. Skonieczny, A. I. Ciuciu, E. M. Nichols, V. Hugues, M. Blanchard-Desce, L. Flamigni and D. T. Gryko, *J. Mater. Chem.*, 2012, **22**, 20649.
68 M. Zhang, M. Li, F. Li, Y. Cheng, J. Zhang, T. Yi and C. Huang, *Dyes Pigm.*, 2008, **77**, 408.
69 Y. X. Yan, Y. H. Sun, L. Tian, H. H. Fan, H. Z. Wang, C. K. Wang, Y. P. Tian, X. T. Tao and M. H. Jiang, *Opt. Mater.*, 2007, **30**, 423.
70 Y. F. Sun, W. Huang, C. G. Lu and Y. P. Cui, *Dyes Pigm.*, 2009, **81**, 10.
71 Y. X. Yan, H. H. Fan, C. K. Lam, H. Huang, J. Wang, S. Hu, H. Z. Wang and Z. M. Chen, *Bull. Chem. Soc. Jpn.*, 2006, **79**, 1614.
72 N. Lin, X. Zhao, J. X. Yang, M. H. Jiang, J. C. Liu, C. K. Wang, W. Shi, J. Meng and J. Weng, *J. Chem. Phys.*, 2006, **124**, 024704.
73 R. C. M. Ferreira, S. P. G. Costa, H. Goncalves, M. Blesley and M. M. M. Raposo, *New. J. Chem.*, 2017, **41**, 12866.
74 D. Zhang, H. Zhu and X. Sheng, *Phys. Chem. Chem. Phys.*, 2023, **25**, 7508.
75 H. Zhu, D. Zhang, X. Sun, S. Qian, E. Feng and X. Sheng, *Phys. Chem. Chem. Phys.*, 2024, **26**, 12150.
76 W. Feng and Y. Qian, *J. Mater. Chem. B*, 2024, **12**, 2413.
77 L. Shi, Z. Sun, N. Richy, M. Blanchard-Desce, O. Mongin, F. Paul and C. O. Paul-Roth, *Chem. Eur. J.*, 2024, **30**, e202303243.
78 M. Durko-Maciag, G. Ulrich, J. Massue, J. Mysliwiec and K. Cyprych, *Eur. Pol. J.*, 2023, **195**, 112235.
79 T. Wloka, M. Gottschaldt and U. S. Schubert, *Chem. - Eur. J.*, 2022, **28**, e202104191.
80 D. Cvejn, E. Michail, I. Polyzos, N. Almonasy, O. Pytela, M. Klikar, T. Mikysek, V. Giannetas, M. Fakis and F. Bureš, *J. Mater. Chem. C*, 2015, **3**, 7345.
81 D. Cvejn, E. Michail, K. Seintis, M. Klikar, O. Pytela, T. Mikysek, N. Almonasy, M. Ludwig, V. Giannetas, M. Fakis and F. Bureš, *RSC Adv.*, 2016, **6**, 12819.
82 M. Klikar, D. Georgiou, I. Polyzos, M. Fakis, Z. Růžičková, O. Pytela and F. Bureš, *Dyes Pigm.*, 2022, **201**, 110230.
83 F. Kournoutas, A. Fihey, J. P. Malval, A. Spangenberg, M. Fecková, P. le Poul, C. Katan, F. Robin-le Guen, F. Bureš, S. Achelle and M. Fakis, *Phys. Chem. Chem. Phys.*, 2020, **22**, 4165.
84 S. K. Sachan and G. Anantharaman, *Inorg. Chem.*, 2021, **60**, 9238.
85 M. Klikar, V. Jelínková, Z. Růžičková, T. Mikysek, O. Pytela, M. Ludwig and F. Bureš, *Eur. J. Org. Chem.*, 2017, 2764.
86 J. Kulhánek, O. Pytela, F. Bureš and M. Klikar, *Eur. J. Org. Chem.*, 2021, 3223.
87 T. Szotkowski, F. Bureš, O. Pytela, J. Kulhánek and Z. Trávníček, *J. Heterocycl. Chem.*, 2006, **43**, 1583.
88 E. Novotná, I. V. Kityk, O. Pytela, F. Bureš, M. Ludwig, M. Klikar, K. Ozga and J. Jedryka, *Chem. Plus. Chem.*, 2020, **85**, 1549.
89 N. Zhang, C. Zeng, C. M. Lam, R. K. Gbur and R. D. Little, *J. Org. Chem.*, 2013, **78**, 2104.
90 K. Y. Zhang, N. Lu, S. J. Yoo, L. M. Hu, R. D. Little and C. C. Zeng, *Electrochim. Acta*, 2016, **199**, 357.
91 T. J. Carter, R. Mohtadi, T. S. Arthur, F. Mizuno, R. Zhang, S. Shirai and J. W. Kampf, *Angew. Chem. Int. Ed.*, 2014, **53**, 3173.
92 A. A. Isse and A. Gennaro, *J. Phys. Chem. B*, 2010, **114**, 7894.
93 D. T. Sawyer, A. Sobkowiak and J. L. Roberts, *Electrochemistry for Chemists*, J. Wiley and Sons Inc, 2nd edn, 1995, ISBN: 978-0-471-59468-0.
94 A. M. Brouwer, *Pure Appl. Chem.*, 2011, **83**, 2213.
95 V. Gopi, S. Subbiahraj, K. Chemmanghattu and P. C. Ramamurthy, *Dyes Pigm.*, 2020, **173**, 107887.
96 J. E. Barnsley, W. Pelet, J. McAdam, K. Wagner, P. Hayes, D. L. Officer, P. Wagner and K. C. Gordon, *J. Phys. Chem. A*, 2019, **123**, 5957.
97 M. Fakis, V. Petropoulos, P. Hrobárik, J. Nociarová, P. Osuský, M. Maiuri and G. Cerullo, *J. Phys. Chem. B*, 2022, **126**, 8532.
98 A. Cesaretti, T. Bianconi, M. Coccimiglio, N. Montegiove, Y. Rout, P. L. Gentili, R. Misra and B. Carlotti, *J. Phys. Chem. C*, 2022, **126**, 10429.
99 J. C. Collings, S. Y. Poon, C. Le Droumaguet, M. Charlot, C. Katan, L. O. Pålsson, A. Beeby, J. A. Mosely, H. M. Kaiser, D. Kaufmann, W. Y. Wong, M. Blanchard-Desce and T. B. Marder, *Chem. - Eur. J.*, 2009, **15**, 198.
100 N. S. Makarov, S. Mukhopadhyay, K. Yesudas, J. L. Brédas, J. W. Perry, A. Pron, M. Kivala and K. Müllen, *J. Phys. Chem. A*, 2012, **116**, 3781.
101 M. G. Vivas, D. L. Silva, J. Malinge, M. Boujtita, R. Zalesny, W. Bartkowiak, H. Angren, S. Canuto, L. De Boni, E. Ishow and C. R. Mendonca, *Sci. Rep.*, 2014, **4**, 4447.
102 A. Rebane, M. Drobizhev, N. S. Makarov, E. Beuerman, S. Tillo and T. Hughes, *J. Lumin.*, 2010, **130**, 1619.
103 A. Rebane, M. Drobizhev, N. S. Makarov, E. Beuerman, J. E. Haley, D. M. Krein, A. R. Burke, J. L. Flikkema and T. M. Cooper, *J. Phys. Chem. A*, 2011, **115**, 4255.
104 M. J. Frisch, G. W. Trucks, H. B. Schlegel, G. E. Scuseria, M. A. Robb and J. R. Cheeseman, *et al.*, *Gaussian 16*, Wallingford, CT, 2016.
105 H. J. Womer, C. A. Arrell, N. Banerji, A. Gennizzo, M. Chergui and A. K. Das, *et al.*, *Struct. Dyn.*, 2017, **4**, 061508.
106 R. Misra and S. P. Bhattacharyya, *Intramolecular Charge Transfer: Theory and Applications*, Wiley-VCH Verlag GmBH & Co, 2018, Germany.
107 P. K. Samanta and S. R. Misra, *J. Appl. Phys.*, 2023, **133**, 020901.

